Fluctuating interfaces in microemulsion and sponge phases

G. Gompper and J. Goos
Sektion Physik der Ludwig-Maximilians-Universität München, Theresienstrasse 37, 80333 München, Germany
(Received 28 March 1994)

A simple Ginzburg-Landau theory with a single, scalar order parameter is used to study the microscopic structure of microemulsions and sponge phases. The scattering intensity in both film and bulk contrast, as well as averages of the internal area S, the Euler characteristic χ_E, and the mean curvature squared $\langle H^2 \rangle$, are calculated by Monte Carlo methods. The results are compared with results obtained from a variational approach in combination with the theory of Gaussian random fields and level surfaces. The results for the location of the transition from the microemulsion to oil-water coexistence, for the scattering intensity in bulk contrast, and for the dimensionless ratio $\chi_E V^2/S^3$ (where V is the volume) are found to be in good quantitative agreement. However, the variational approach fails to give a peak in the scattering intensity in film contrast at finite wave vector, a peak which is observed both in the Monte Carlo simulations and in experiment. Also, the variational approach fails to produce a transition from the microemulsion to the lamellar phase.

PACS number(s): 82.70.−y, 05.40.+j, 61.20.Gy

I. INTRODUCTION

The understanding of binary and ternary amphiphilic systems has made considerable progress over the last few years [1,2]. One of the phases which has received particular attention is the microemulsion, a homogeneous, isotropic mixture of oil, water, and amphiphile. It is by now well established that the microemulsion consists of homogeneous regions of oil and water, which form a complicated, intertwined network, with a typical length scale of a few hundred Å. This is possible because the amphiphile forms a monolayer at the interface between these oil and water regions and thereby reduces the interfacial tension, so that a phase with an extensive amount of internal interface can become stable. The structure of the sponge phase in aqueous surfactant solutions is very similar [3,4]. In this case an amphiphilic bilayer separates two multiply connected water networks.

In order to characterize the internal structure of a microemulsion, several quantities have been proposed. Most experiments and theoretical studies have concentrated on the water-water correlation function, or equivalently the scattering intensity in bulk contrast [1,2]. However, a two-point correlation function gives little information about the connectivity and percolation of the oil and water networks in a microemulsion. The latter property can be probed by conductivity and diffusion experiments. From a theoretical point of view, the topology of a microemulsion can be characterized by its Euler characteristic [5–8], a quantity which unfortunately is difficult to measure experimentally [7].

We want to investigate here a simple Ginzburg-Landau model for oil-water-amphiphile mixtures [9,10]. This model has been used previously to calculate the spectrum of capillary waves of an oil-water interface [10,11], to explain the wetting behavior of the microemulsion at the oil-water interface [10,12,13], to describe several ordered phases such as a lamellar, a hexagonal, and a cubic phase [14], and to study the behavior of amphiphilic systems in confined geometry [11,15]. The same model has also been used to predict sound attenuation and dispersion in microemulsions [16]. In Ref. [17], this model has been studied by Monte Carlo simulations. It has been shown that there is a region in the phase diagram where the microemulsion is stabilized by thermal fluctuations. This is the part of the phase diagram we want to investigate here in more detail. In particular, simulations are used to calculate the scattering intensity both in bulk and film contrast, and the geometrical quantities area, Euler characteristic, and the mean curvature squared. The results are then compared with the results obtained from a simple variational calculation and from a self-consistent perturbation theory.

The variational approach has been applied recently to calculate the scattering intensity of an ensemble of random interfaces with bending rigidity [18]. To make the random interface model accessible to the variational method, a mean-spherical approximation has been used as a first step. In comparison to that model, we are here in a position that we can directly compare the results obtained from the variational approach with the results of our Monte Carlo simulation, and thus check the quality of this approximation.

II. GINZBURG-LANDAU MODEL

Our analysis is based on the free-energy functional [10]

$$\mathcal{F}\{\Phi\} = \int d^3r \ \left[c(\Delta\Phi)^2 + g(\Phi)(\nabla\Phi)^2 + f(\Phi) - \mu\Phi\right] \tag{1}$$

for a single, scalar order parameter field $\Phi(\mathbf{r})$, which is proportional to the local difference of the oil and water concentrations. Here, μ is the chemical potential difference between oil and water. The amphiphile concentra-

tion does not appear explicitly in our model, and should be considered to be integrated out [19]. The average amphiphile concentration enters the model (1) via the parameters of the functions f and g, which are chosen to take the form [17]

$$f(\Phi) = \omega(\Phi - \Phi_o)^2(\Phi^2 + f_0)(\Phi - \Phi_w)^2, \quad (2)$$

$$g(\Phi) = g_0 + g_2\Phi^2 . \quad (3)$$

With this choice for f and g, a three-phase coexistence between a oil-rich phase with $\langle\Phi\rangle \simeq \Phi_o$, a water-rich phase with $\langle\Phi\rangle \simeq \Phi_w$, and a microemulsion with $\langle\Phi\rangle \simeq 0$ can be described. We consider here only systems with oil-water symmetry, where $\Phi_o = -\Phi_w \equiv \Phi_b$. The constant f_0 in Eq. (2) is proportional to the chemical potential of the amphiphile, while g_0 decreases with increasing amphiphile strength or amphiphile concentration [20]. The value of g_0 determines the behavior of correlation function $G(r) = \langle\Phi(\mathbf{r})\Phi(0)\rangle$, and of the scattering intensity in bulk contrast [9,10]. For g_0 sufficiently small or negative, the correlation function in the microemulsion decays with damped oscillations, while the scattering intensity has a peak at nonzero wave vector k. To ensure a monotonic decay of $G(r)$ in the oil-rich and water-rich phases, we choose

$$g_2 = 4\sqrt{1 + f_0} - g_0 + 0.01 . \quad (4)$$

The natural length scale of the model (1), (2), and (3) is [12]

$$\ell_0 = \left(\frac{c}{\omega\Phi_b^4}\right)^{1/4} . \quad (5)$$

For all explicit calculations, we use the parameter set $c = 1$, $\omega = 1$, $\Phi_b = 1$, and $\mu = 0$; this implies in particular $\ell_0 = 1$. Thus, we study the microemulsion structure as a function of the parameters f_0 and g_0.

The same model can also be interpreted as a model for binary amphiphilic systems [4,21–23], if the amphiphilic molecules form bilayers without holes or seams. The bilayers separate space into an "inside" ($\Phi > 0$) and an "outside" ($\Phi < 0$). In this case, the microemulsion phase corresponds to the symmetric sponge phase, and the oil-rich and water-rich phases to the asymmetric droplet phase.

III. METHODS

A. Monte Carlo simulations

To study the field-theoretic model (1) by Monte Carlo simulations, space has to be discretized by introducing a simple cubic $N \times N \times N$ lattice with lattice constant a_0 (and periodic boundary conditions). However, the order-parameter field $\Phi(\mathbf{r}_i)$ at each lattice site i is still a continuous, real variable. Details about the simulation procedure, about the triangulation of the $\Phi(\mathbf{r}) = 0$ surface, and about the calculation of the area can be found in Ref. [17]. In addition to the quantities [25] studied in Ref. [17], we also calculate here the mean curvature squared and the scattering intensity in film contrast.

The calculation of the film scattering is rather straightforward. As in models for level surfaces and Gaussian random fields, we define the film scattering intensity as the Fourier transform of the correlation function

$$G_{\rm film}(r;\epsilon) = N_0\langle\delta_\epsilon(\Phi(\mathbf{r}))\delta_\epsilon(\Phi(0))\rangle, \quad (6)$$

where $\delta_\epsilon(x) = 1/\epsilon$ for $-\epsilon/2 \le x \le +\epsilon/2$, and zero otherwise. The normalization factor N_0 is chosen such that $\lim_{r\to\infty} G_{\rm film}(r;\epsilon) = 1$. This correlation function is proportional to the probability distribution to find two points at distance r in a thin layer of thickness ϵ of the $\Phi = 0$ surface. In the simulations, we calculate the distance distribution of lattice sites for which $|\Phi(\mathbf{r})| \le \epsilon/2$ (with periodic boundary conditions).

To calculate the mean curvature, we consider two neighboring triangles j and k. Let b_{jk} be their common edge, U_j and U_k their perimeters, and S_j and S_k their areas. Each triangle has a normal vector $\mathbf{n}$ pointing towards the oil. For the calculation of the radius of curvature, we have to assume that the two triangles are approximately equilateral. The radius of the sphere, which touches both triangles in their centers of mass, is then taken to be the radius of curvature,

$$|R_{jk}| = 3^{-3/4}\left(\frac{S_j + S_k}{2}\right)^{1/2}\left(\frac{2 - \mathbf{n}_j\cdot\mathbf{n}_k}{\mathbf{n}_j\cdot\mathbf{n}_k}\right)^{1/2} . \quad (7)$$

The sign of R_{jk} is easily obtained from the two normal vectors, and the vector connecting the centers of mass of the two triangles. The mean curvature c_j of the whole triangle j is obtained by a sum over the contributions from the edges with the three neighboring triangles k_1, k_2, and k_3, weighted with the lengths of these edges,

$$c_j = \frac{1}{U_j}\sum_{i=1}^{3}\frac{b_{jk_i}}{R_{jk_i}} . \quad (8)$$

We want to point out that it is essential to define the mean curvature on triangles rather than on edges, because only in this way can the mean curvature near saddle points be described correctly.

The total mean curvature and the total mean curvature squared are then sums over all triangles,

$$\int dS\ H = \frac{2}{\sqrt{3}}\sum_j S_j c_j, \quad (9)$$

$$\int dS\ H^2 = \frac{2}{\sqrt{3}}\sum_j S_j c_j^2 , \quad (10)$$

where the integral is over the whole surface. The additional factor $2/\sqrt{3}$ is obtained by triangulating the surface of a sphere and comparing the results (9) and (10) with the exact results in the limit of large sphere radius. A similar procedure has been used in Refs. [26] and [27].

In order to test the quality of these expressions, we have calculated the (average) mean curvature and mean curvature squared for spheres and cylinders, as a function

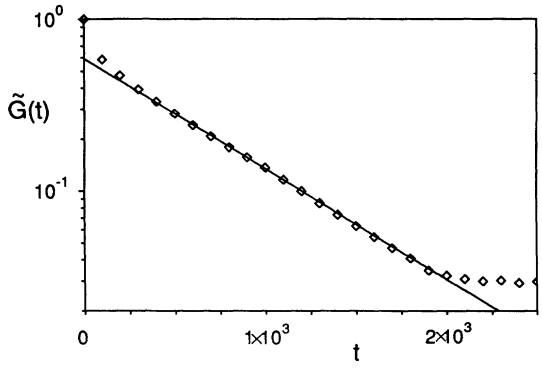

FIG. 1. Auto-correlation function, $\tilde{G}(t)$, as a function of time t (in units of Monte Carlo steps per site), for the parameters $g_0 = -2$ and $f_0 = 0.5$ ($N = 27$, $a_0 = 0.8\ell_0$).

of the radius R. For $R > 2a_0$, where a_0 is the lattice constant, the agreement with the exact results is very good, with deviations of only a few percent. We have also studied corrugated surfaces (with saddle points), which are given by the Monge parametrization

$$z(x,y) = z_0 \sin(2\pi x/L)\sin(2\pi y/L).$$

In this case, the deviations are less than a few percent for $L > 6a_0$ with $z_0 = a_0$, and for $L > 9a_0$ with $z_0 = 3a_0$.

An important question in any Monte Carlo simulation is whether the system has reached thermal equilibrium. To answer this question, we have calculated the auto-correlation function [28] in thermal equilibrium, as a function of Monte Carlo time t,

$$\tilde{G}(t) = \frac{\sum_{i=1}^{N^3} \left[\langle \Phi(\mathbf{r}_i,t)\Phi(\mathbf{r}_i,0)\rangle - \langle\Phi(0,0)\rangle^2\right]}{N^3\left[\langle\Phi(0,0)^2\rangle - \langle\Phi(0,0)\rangle^2\right]}, \quad (11)$$

where N^3 is the number of lattice sites. The exponential decay of this function gives us the relaxation time τ. The result for $\tilde{G}(t)$ for our model in the microemulsion, near the point of four-phase coexistence of oil-rich, water-rich, microemulsion, and lamellar phases, is shown in Fig. 1. It shows that the relaxation time is $\tau \simeq 680$ [in units of Monte Carlo steps per lattice site (MCS)]. Since in our simulations we usually average over 50 000 to 100 000 MCS, all our results represent true equilibrium averages.

B. Variational approach

The variational method [29] introduces a Gaussian model with the free-energy functional

$$\mathcal{F}_0\{\Phi\} = \int d^3r \int d^3r' \times[\Phi(\mathbf{r}) - \overline{\Phi}]\, G_0^{-1}(|\mathbf{r}-\mathbf{r}'|)\,[\Phi(\mathbf{r}') - \overline{\Phi}]\,. \quad (12)$$

Then the Feynman-Bogoliubov inequality

$$F \le F_u \equiv F_0 + \langle \mathcal{F} - \mathcal{F}_0\rangle_0 \quad (13)$$

is used to construct an upper bound for the free energy F of the system described by the functional $\mathcal{F}$. Here, both the free energy F_0 and the average $\langle\ldots\rangle_0$ are calculated with the free-energy functional (12). In Eqs. (12) and (13), a cutoff Λ in momentum space is implicit. In order to compare with the results of the Monte Carlo simulations, we set $\Lambda = 2\pi/(\gamma_0 a_0)$, where a_0 is the lattice constant used in the simulations, and $\gamma_0 \simeq 1$. The best approximation to F in this approach is then obtained by minimizing F_u with respect to G_0 and $\overline{\Phi}$. For the free-energy functional (1) with (2) and (3), we find

$$F_u = 15\omega G_0(r=0)^3 + A_2 G_0(r=0)^2 + A_1 G_0(r=0) + A_0 + \int \frac{d^3k}{(2\pi)^3}\left\{G_0(k)\left[ck^4 + (B + g_2 G_0(r=0)k^2)\right] - \frac{1}{2}\ln\left(G_0(k)\right)\right\}, \quad (14)$$

where

$$A_2 = 3\omega(15\overline{\Phi}^2 + f_0 - 2\Phi_b^2), \quad (15)$$

$$A_1 = \omega\left[15\overline{\Phi}^4 + 6(f_0 - 2\Phi_b^2)\overline{\Phi}^2 + (\Phi_b^2 - 2f_0)\Phi_b^2\right], \quad (16)$$

$$A_0 = \omega(\overline{\Phi}^2 + f_0)(\overline{\Phi}^2 - \Phi_b^2)^2, \quad (17)$$

$$B = g_0 + g_2\overline{\Phi}^2\,. \quad (18)$$

The optimal Gaussian correlation function is obtained by requiring that the functional derivative of F_u with respect to $G_0(k)$ must vanish, which implies

$$[45\omega G_0(r=0)^2 + 2A_2 G_0(r=0) + A_1] + [B + g_2\langle k^2\rangle]k^2 + ck^4 - \frac{1}{2G_0(k)} = 0\,, \quad (19)$$

where $\langle k^2\rangle$ is the second moment of $G_0(k)$ in Fourier space. Thus, the correlation function in the variational approach has the Teubner-Strey form [9]

$$G_0(k)^{-1} = 2(b_0 + b_2k^2 + ck^4)\,, \quad (20)$$

with constants b_0 and b_2. Its Fourier transform is given by [9]

$$G_0(r) = A\frac{1}{r}e^{-r/\xi}\sin qr \quad (21)$$

where ξ is the correlation length, with

$$\xi^{-2} = \frac{1}{2}\sqrt{\frac{b_0}{c}} + \frac{1}{4}\frac{b_2}{c}\,, \quad (22)$$

$2\pi/q$ is the average domain size of coherent oil and water regions, with

$$q^2 = \frac{1}{2}\sqrt{\frac{b_0}{c}} - \frac{1}{4}\frac{b_2}{c}\,, \quad (23)$$

and

$$A = \frac{\xi}{16\pi cq} . \tag{24}$$

The correlation function (20) in combination with the theory of Gaussian random fields [30–32] can then be used to calculate the film scattering intensity, and the film area (per unit volume) S/V, the mean curvature squared $\langle H^2 \rangle$, and the Euler characteristic (per unit area) χ_E/S. For a film of thickness ϵ, the film scattering intensity is found to be [32]

$$G^{(0)}_{\rm film}(r;\epsilon) = \frac{N_0}{2\pi\langle\Phi^2\rangle} \frac{1}{\sqrt{1-g(r)^2}} \int_{-\infty}^{+\infty} ds \int_{-\infty}^{+\infty} dt \times \exp\left[-\frac{s^2+t^2-2g(r)st}{2\langle\Phi^2\rangle[1-g(r)^2]}\right] \delta_\epsilon(s)\delta_\epsilon(t), \tag{25}$$

where $g(r) \equiv G_0(r)/G_0(r=0)$. In the limit $\epsilon \to 0$, this expression simplifies to

$$G^{(0)}_{\rm film}(r) = \frac{1}{\sqrt{1-g(r)^2}} , \tag{26}$$

or explicitly, with (21),

$$G^{(0)}_{\rm film}(r) = \left[1 - \exp(-2r/\xi)\frac{\sin(qr)^2}{(qr)^2}\right]^{-1/2} . \tag{27}$$

Thus, the film correlation function diverges as $G^{(0)}_{\rm film}(r) \sim \sqrt{\xi/r}$ for $r \to 0$. Note that it follows immediately from Eq. (26) that $G^{(0)}_{\rm film}(r) \geq G^{(0)}_{\rm film}(r=\infty)$.

To obtain the geometrical quantities, we employ the exact results [31] for $\Phi(\mathbf{r}) = \overline{\alpha}$ surfaces of Gaussian random fields with $\langle\Phi\rangle = 0$ [33],

$$S/V = \frac{2}{\sqrt{3}\pi}\sqrt{\langle k^2\rangle}\ \exp\left(-\frac{\alpha^2}{2}\right), \tag{28}$$

$$\chi_E/S = \frac{1}{12\pi}\langle k^2\rangle(\alpha^2-1), \tag{29}$$

$$\langle H\rangle = \frac{\sqrt{\pi}}{2\sqrt{6}}\sqrt{\langle k^2\rangle}\alpha, \tag{30}$$

$$\langle H^2\rangle = \frac{1}{6}\langle k^2\rangle\left(\frac{6}{5}\frac{\langle k^4\rangle}{\langle k^2\rangle^2} + \alpha^2 - 1\right), \tag{31}$$

where $\alpha = \overline{\alpha}/\sqrt{G_0(r=0)}$. Here, $\langle k^2\rangle$ and $\langle k^4\rangle$ are the second and fourth moments of the correlation function $G_0(k)$ in Fourier space.

C. Self-consistent perturbation theory

Another method to calculate correlation functions beyond the Ornstein-Zernike (OZ) approximation is a perturbation in the higher-than-quadratic terms in (1) with (2) and (3). The two-point correlation function can be expressed by the Dyson equation,

$$G(k)^{-1} = G_{\rm OZ}(k)^{-1} - \Sigma(k) \tag{32}$$

in terms of the self-energy $\Sigma(k)$. Here,

$$G_{\rm OZ}(k)^{-1} = 2(ck^4 + g_0k^2 + \omega) \tag{33}$$

is the bare propagator. The self-energy $\Sigma(k)$ can now be expressed in terms of the full propagator $G(k)$, and the full four-point and six-point vertex functions $\Gamma^{(4)}(k)$ and $\Gamma^{(6)}(k)$. The Feynman diagrams are shown in Fig. 2(a). To proceed, we need an expression for the vertex functions. This can only be done approximately. The simplest approximation is to use the bare vertex functions [see Eqs. (1), (2), and (3)]

$$\Gamma^{(4)}_{\rm bare}(k_1,k_2,k_3,k_4) = 24\left[\frac{g_2}{12}(k_1^2+k_2^2+k_3^2+k_4^2) + \omega(f_0 - 2\Phi_b^2)\right] \times\delta(k_1+k_2+k_3+k_4), \tag{34}$$

$$\Gamma^{(6)}_{\rm bare}(k_1,k_2,k_3,k_4,k_5,k_6) = 720\omega\ \delta(k_1+k_2+k_3+k_4+k_5+k_6) . \tag{35}$$

The Dyson Eq. (32) is then solved self-consistently. This is the approximation used in Ref. [34] to calculate the scattering intensity for a Ginzburg-Landau model (1) with $g_2 = 0$ in Eq. (3) and $f(\Phi) = t\Phi^2 + v\Phi^4$. In our case, it gives very bad results in the region of the phase diagram, where strongly structured microemulsions are stable (neither the peak position nor the peak intensity are consistent with the Monte Carlo data). The simple approximation can be improved by calculating the vertex functions self-consistently. We include all Feynman diagrams up to two-loop order, as shown in Figs. 2(b) and 2(c), where again all internal lines correspond to the full propagator $G(k)$. In addition, we expand the vertex functions in powers of k, and truncate this series after

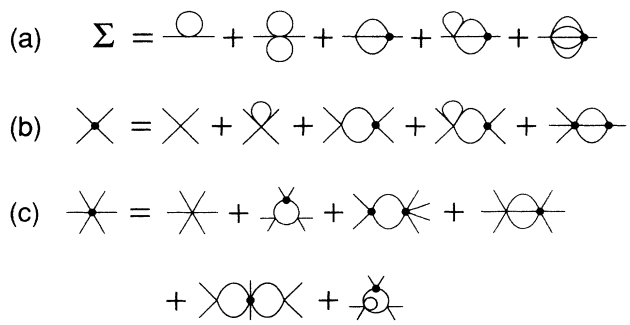

FIG. 2. (a) Dyson equation for the self-energy Σ. (b) Two-loop expansion of the vertex function $\Gamma^{(4)}$. (c) Two-loop expansion of the vertex function $\Gamma^{(6)}$. In these Feynman diagrams, the full lines indicate the full propagator $G(\mathbf{k})$; vertices without a circle are the bare vertex functions $\Gamma^{(4)}_{\rm bare}$ and $\Gamma^{(6)}_{\rm bare}$, vertices with a full circle denote the renormalized vertex functions.

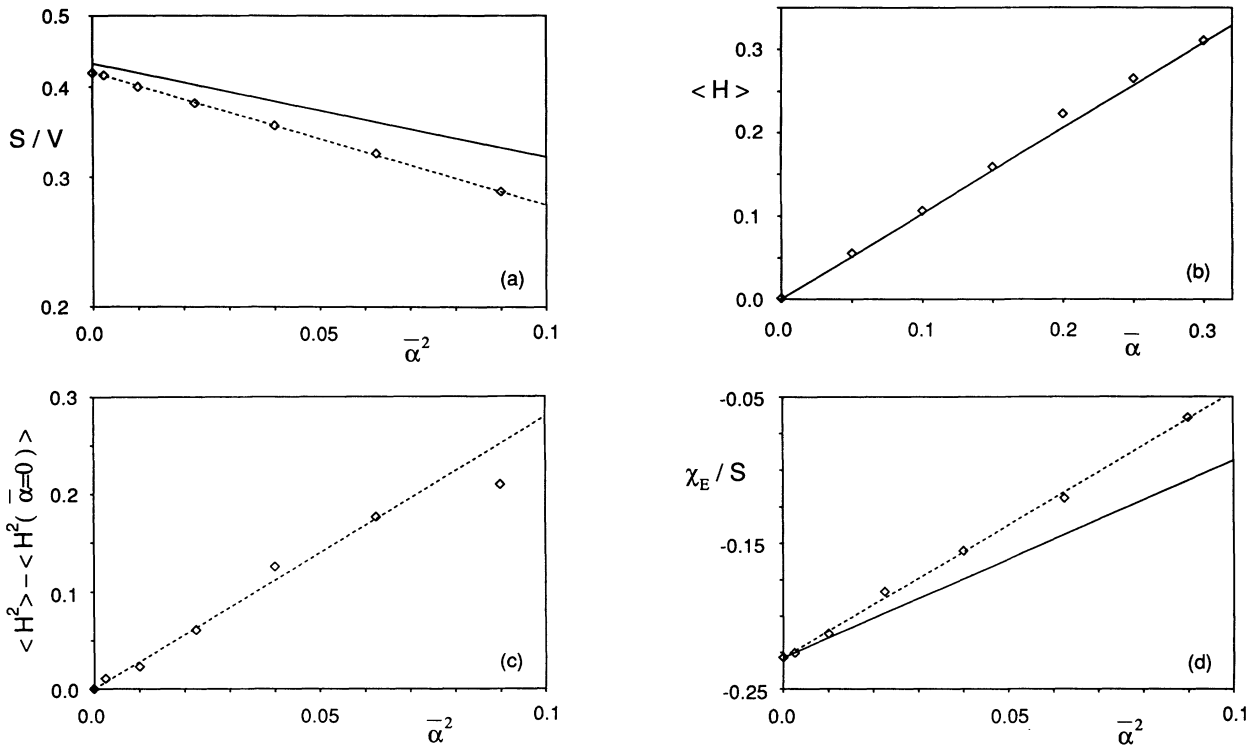

FIG. 3. (a) Area (per unit volume), S/V, (b) average mean curvature $\langle H \rangle$, (c) average mean curvature squared $\langle H^2 \rangle$, and (d) Euler characteristic (per unit area), χ_E/S, of level surfaces of Gaussian random fields. Note the logarithmic scale of the ordinate in (a). The dashed lines are linear fits of the Monte Carlo data ($N = 27$, $a_0 = 0.8\ell_0$). The full lines are the exact results of the continuum model with cutoff parameter $\gamma_0 = 2.5$.

the first few terms, such that the form of the free-energy functional (1), (2), and (3) is recovered after each step. The resulting equations are solved numerically.

IV. GAUSSIAN RANDOM FIELDS

In order to test our numerical procedures, we have simulated a model for Gaussian random surfaces, with $g_2 = 0$ in Eq. (3), and

$$f(\Phi) = \omega \Phi^2 \ . \tag{36}$$

In this case, the exact results for level surfaces in the continuum model are given by Eqs. (28), (29), (30), and (31). Our numerical results are shown in Fig. 3. In all four cases the linear or quadratic dependence on α is reproduced very well. We have also calculated the prefactors from Eqs. (28), (29), and (30). Note that $\langle k^2 \rangle$ has a strong cutoff dependence, and $\langle k^4 \rangle$ even more so. For the cutoff parameter $\gamma_0 = 2.5$, we obtain the full lines in Fig. 3. In the case of $\langle H \rangle$, the agreement is excellent. For S/V and χ_E/S, there is an appreciable deviation for large values of $\bar{\alpha}$. This is not very surprising, since the structures get very small in this case, and thus cannot be described very well by our triangulation procedure. For $\langle H^2 \rangle$, the amplitude of α^2 in Fig. 3(c) is about a factor of 2 too large compared to Eq. (31).

Equations (28), (29), and (30) can be used to obtain a relation between S/V, χ_E, and $\langle H \rangle$, which is *independent* of α and $\langle k^2 \rangle$, and thus does not depend on any cutoff. One easily finds that

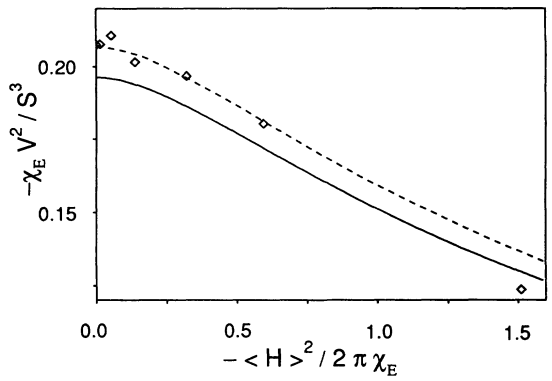

FIG. 4. The scaled Euler characteristic, $-\chi_E V^2/S^3$, as a function of the scaled mean curvature $-\langle H \rangle^2 S/(2\pi\chi_E)$, of level surfaces of Gaussian random fields. The diamonds are the Monte Carlo data, the full line is the exact result (38). For a better comparison of the shape of the two curves, we also show the exact result multiplied by a factor of 1.053 (dashed line).

$$-\frac{\chi_E V^2}{S^3} = \frac{\pi}{16}\,\Theta\left(-\frac{\langle H\rangle^2 S}{2\pi\chi_E}\right) \tag{37}$$

with $\Theta(0) = 1$, where the scaling function Θ is given by

$$\Theta(x) = \frac{\pi}{\pi + 4x}\,\exp\left(\frac{4x}{\pi + 4x}\right) . \tag{38}$$

A comparison of the Monte Carlo data for the Gaussian model with the scaling form (37) is shown in Fig. 4. The agreement in this case is very good, with deviations of only a few percent.

V. PHASE DIAGRAM

The phase diagram of our Ginzburg-Landau model, calculated in the mean-field approximation, by Monte Carlo simulations [17], and with the variational method, is shown in Fig. 5. The results of the variational approach depend on the choice of the cutoff $\Lambda = 2\pi/(\gamma_0 a_0)$. We have determined γ_0 from a fit of the scattering intensity to the Monte Carlo data at *one* point in the phase diagram (see discussion below), which gives $\gamma_0 = 1.5$. It can be seen in Fig. 5 that with this value of γ_0, the variational result for the location of the line of phase transitions from oil-water coexistence to the microemulsion or lamellar phase reproduces the qualitative behavior of the Monte Carlo data very well; the quantitative agreement is not perfect, but much better than the mean-field result.

The lamellar phase cannot be studied with the variational ansatz (12) with an isotropic correlation function G_0. Thus, to detect a transition from the microemulsion to a spatially ordered phase, we are looking for a spinodal, where the scattering intensity $G_0(k)$ diverges at some nonzero value of the wave vector k. Much to our surprise, no such spinodal exists. A closer look at the structure of Eq. (19) reveals that this is not a numerical problem. Since $G_0(r = 0) = \xi/(16\pi c)$ [see Eqs. (21) and (24)], the behavior of $G_0(k)$ for large ξ (where $\langle k^2\rangle \simeq q^2$) is given by

$$G_0(k) \simeq \frac{1}{2[ck^4 + (g_0 + r_2)k^2 + r_0\xi^2]} , \tag{39}$$

with constants r_0 and r_2. From a calculation similar to that leading to Eq. (22), one finds that the spinodal is located at $g_0 + r_2 = -\sqrt{4cr_0}\xi$. Thus, $\xi \to \infty$ implies $g_0 \to -\infty$.

However, there is a strong peak in the variational scattering intensity at some nonzero wave vector, which sharpens and increases in height as the system is taken from the microemulsion phase into a region of the phase diagram, where the lamellar phase is found in the Monte Carlo simulations. Thus, in order to get an estimate for the transition line, we use a Lindemann type criterion [35] by requiring that the dimensionless product $q\xi$ equal some fixed value w at the transition. We use here $w = 5$; this choice is motivated by the fact that values of $q\xi \gtrsim 5$ have been observed neither experimentally [9,36,37], nor in the simulations of the Ginzburg-Landau model [17]. The result of this approximation is also shown in Fig. 5. Its qualitative behavior is again in reasonable agreement with the Monte Carlo data. The location of the line of $q\xi = w$ obviously depends on the value of w.

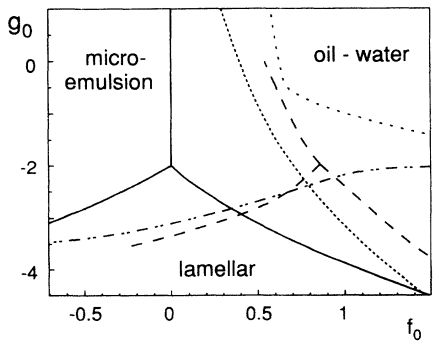

FIG. 5. Phase diagram of the Ginzburg-Landau model (1). Full lines give the mean-field results, dashed lines the Monte Carlo results [17]. In the variational approach, the transition from oil-water coexistence to the microemulsion is indicated by one dotted line (narrow spacing), the spinodal (where the microemulsion looses its metastability) by another dotted line (wide spacing). Finally, the variational estimate of the transition microemulsion lamellar is the dashed-dotted line.

VI. SCATTERING INTENSITIES

The scattering intensity in *bulk* contrast, $G_{\Phi\Phi}(k) = \langle\Phi(\mathbf{k})\Phi(-\mathbf{k})\rangle$, at different points in the phase diagram is shown in Fig. 6. As we have already mentioned in the previous section, the data of Fig. 6(a) have been used to determine the cutoff parameter γ_0 of the variational approach. Note, however, that γ_0 is the only parameter in the fit, which determines the shape *and* the amplitude of the scattering intensity. The same parameter γ_0 is then used to calculate the scattering intensities at other points in the phase diagram, as shown in Fig. 6(b) and 6(c). The agreement with the Monte Carlo data is quite remarkable.

The results of the self-consistent perturbation theory are shown in Fig. 7, at the same points in the phase diagram as in Fig. 6. Given the rather large calculational effort to obtain these curves, the result is rather disappointing. The self-consistent perturbation theory gives only a very weak peak at nonzero wave vector k. Although the position of the peak is roughly correct, the ratio of peak height to the scattering intensity at $k = 0$ varies very little compared to the Monte Carlo data.

The Monte Carlo data for the *film* correlation function in real space are shown in Fig. 8. We find that this correlation shows *oscillations* as a function of distance r. This oscillatory behavior has been observed explicitly so far only in lattice models for microemulsions in one dimension [38–40]. Oscillations are also found in the Gaussian correlation function (27). This correlation function

is also shown in Fig. 8. Two main differences can be recognized immediately: (i) the oscillations of the Monte Carlo data are much more pronounced and (ii) the Monte Carlo data for intermediate r drop below the asymptotic value of $G_{\rm film}$ for $r \to \infty$, while the Gaussian correlation function does not (as discussed above). These two differences have important consequences when the film scattering intensity is calculated (by a numerical Fourier transform of the data shown in Fig. 8). The results for this scattering intensity are shown in Fig. 9(a). Note that while the variational correlation function decays monotonically, the Monte Carlo result displays a small peak at some nonzero value of the wave vector k. The latter behavior is just what is seen in experiment [41–43].

The Fourier transform of Eq. (27) depends on a single parameter, the dimensionless product $q\xi$. We can thus ask if the Gaussian scattering intensity in film contrast shows a peak at nonzero wave vector k for *any* value of $q\xi$ (independent of the value of $q\xi$ obtained by the variational method). The correlation function (27) has its strongest oscillations for large $q\xi$. However, even in the limit $q\xi \to \infty$, no peak or shoulder appears at finite k/q. Thus, the Gaussian scattering intensity in film contrast *never* has a peak at finite wave vector k.

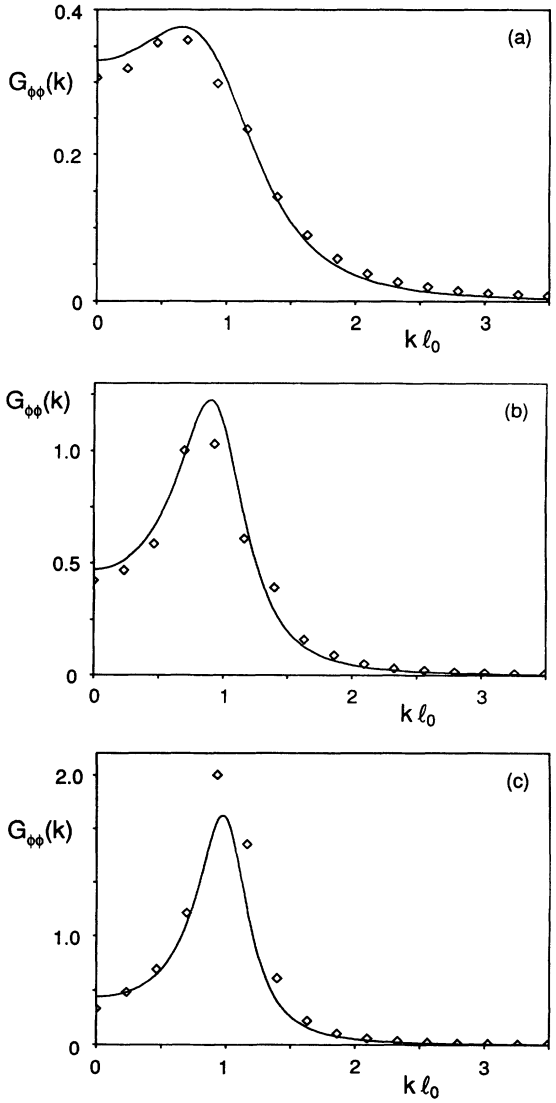

FIG. 6. Scattering intensity in bulk contrast. The full lines are the results of the variational approach, the diamonds are the Monte Carlo data ($N = 45$, $a_0 = 0.6\ell_0$). (a) $g_0 = -1.0$, $f_0 = 0.0$. The data at this point in the phase diagram are used to determine the cutoff parameter $\gamma_0 = 1.5$. (b) $g_0 = -2.0$, $f_0 = 0.5$. (c) $g_0 = -2.5$, $f_0 = 0.675$.

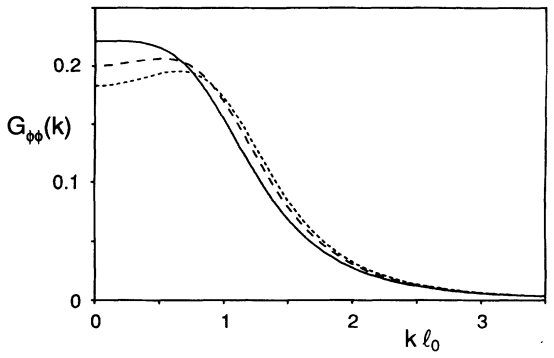

FIG. 7. Scattering intensity in bulk contrast as obtained from the self-consistent screening approximation. The parameters are $g_0 = -1.0$, $f_0 = 0.0$ (full line), $g_0 = -2.0$, $f_0 = 0.5$ (dashed line), and $g_0 = -2.5$, $f_0 = 0.675$ (dotted line).

An analytical expression for the film scattering intensity has been obtained recently from a Ginzburg-Landau model with two scalar order-parameter fields [4,22,23], the concentration difference between oil and water, $\Phi(\mathbf{r})$, and the amphiphile concentration, $\rho(\mathbf{r})$. In this case, one finds for the amphiphile-amphiphile correlation function [23]

$$G_{\rho\rho}(k) = \frac{\chi_\rho}{1+(k\xi_\rho)^2} + \left(\frac{\chi_\rho}{1+(k\xi_\rho)^2}\right)^2 \Gamma(k\xi, q\xi), \quad (40)$$

where

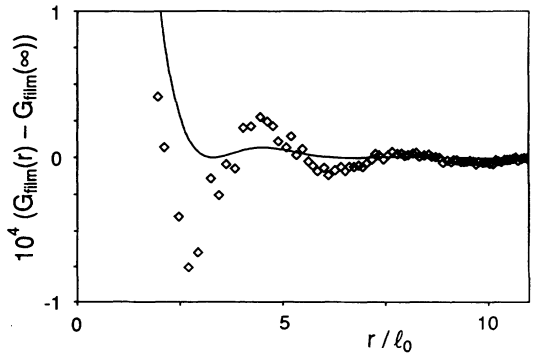

FIG. 8. Film correlation function $G_{\rm film}(r)$ in real space, for $g_0 = -2.5$ and $f_0 = 0.675$, with film thickness $\epsilon = 0.1\Phi_b$. The full line is the variational result (with $\gamma_0 = 1.5$), the Monte Carlo data ($N = 27$, $a_0 = 0.8\ell_0$) are given by diamonds.

$$\chi_\rho\,\Gamma(x,y) = (\gamma_1-\gamma_2 x^2)^2\Lambda_-(x,y) + 2\gamma_3(\gamma_1-\gamma_2 x^2)\left[(1-y^2)\Lambda_-(x,y) - y\Xi(x,y)\right] + \gamma_3^2[2y^2\{(\Lambda_+(x,y)-\Lambda_-(x,y)\} + (1-y^2)^2\Lambda_-(x,y) - 2y(1-y^2)\Xi(x,y) + y^2], \tag{41}$$

with

$$\Lambda_\pm(x,y) = \frac{1}{4x}\left[2\arctan\left(\frac{x}{2}\right) \pm \arctan\left(\frac{4x}{4+4y^2-x^2}\right) \pm n\pi\right] \tag{42}$$

$$\Xi(x,y) = \frac{1}{4x}\ln\left(\frac{4+(x+2y)^2}{4+(x-2y)^2}\right) . \tag{43}$$

Here, $n = 0$ for $0 \le x^2 < 4+4y^2$ and $n = 1$ for $x^2 > 4+4y^2$. The disadvantage of this two-order-parameter model is that it contains the parameters γ_1, γ_2, γ_3, and ξ_ρ in addition to those which appear in our model (1), (2), and (3). We thus fit the analytic form (40) to our Monte Carlo data, in order to compare the general form of the two results. Here, the value of $q\xi$ is determined from a fit of the Monte Carlo order-parameter correlation function to the Teubner-Strey form (20). The two curves are shown in Fig. 9(b). The agreement is found to be very good for $0 < k/q < 3/2$. This implies in particular that for $1 \ll k\xi \ll q\xi$ the Monte Carlo data show a $1/k$ behavior [4,22,23]. For larger values of k, the expression (40) yields a more rapid decay than the Monte Carlo data. The same discrepancy occurs when (40) is compared with the experimental data, see Ref. [23]. Thus, our Monte Carlo results should describe the experimental behavior even better than the perturbation theory of the two-order-parameter model.

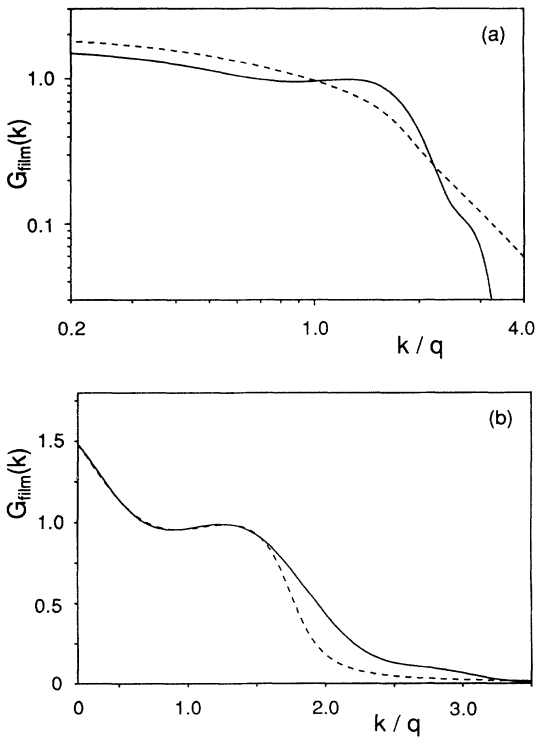

FIG. 9. Scattering intensity in film contrast. The parameters are the same as in Fig. 8. (a) A comparison of Monte Carlo simulation (full line) and the variational approach (dashed line). (b) A comparison of the Monte Carlo data (full line) with the results of the two-order-parameter Landau model, Eq. (40), with $\gamma_1 = 36.1$, $\gamma_2 = -0.21$, $\gamma_3 = 0.53$, and $\xi_\rho/\xi = 0.072$ (dashed line). The value of $q\xi = 9.71$ is obtained by fitting the Monte Carlo results for scattering intensity in bulk contrast to the Teubner-Strey form (20).

VII. STRUCTURE AND TOPOLOGY

A typical configuration of the $\Phi(\mathbf{r}) = 0$ surfaces in a microemulsion near the four-phase point is shown in Fig. 10. Note that fluctuations of the interfaces on length scales *smaller* than the typical domain size are clearly visible. We want to calculate now the area (per unit vol-

FIG. 10. Typical configuration of the $\Phi(\mathbf{r}) = 0$ surfaces in a microemulsion. The parameters are $g_0 = -2.0$, $f_0 = 0.75$, $a_0 = 0.6\ell_0$, and $N = 45$. The figure shows only a part (of size $36\times36\times36$) of the total lattice. The two sides of the interface are colored differently, dark on the oil-rich side, light on the water-rich side.

ume), S/V, the mean curvature squared, $\langle H^2 \rangle$, and the Euler-characteristic (per unit area), χ_E/S [25]. The results of the Monte Carlo simulations are shown in Figs. 11(a), 12(a), and 13(a), and of the variational approach in Figs. 11(b), 12(b), and 13(b). It can be seen that in all three cases the qualitative behavior of the Monte Carlo data is reproduced by the variational results. The best quantitative agreement is found for the Euler characteristic. There is still a reasonable quantitative agreement for the area, while the mean curvature squared is off by about a factor of 3 (which is about the same factor as for Gaussian random fields, see Sec. IV).

We have shown in Sec. IV that the ratio $\chi_E V^2/S^3$ is less sensitive to cutoff effects than the quantities χ_E/S and S/V themselves. Furthermore, it has been shown in Ref. [17] by a simple scaling argument, which is valid beyond Gaussian random fields, that this quantity characterizes the topology of a microemulsion phase *independent* of the domain sizes of the coherent oil and water regions. From the Monte Carlo simulations, this ratio is found to be [17]

$$\frac{\chi_E V^2}{S^3} = -0.176 \qquad \text{(Monte Carlo)} \qquad (44)$$

while for Gaussian random fields, see Eq. (37),

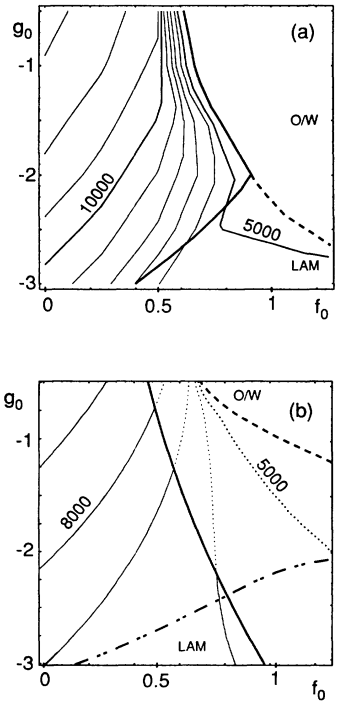

FIG. 11. Contour plot of the area S of internal oil-water interfaces $[\Phi(\mathbf{r}) = 0]$ in the microemulsion or sponge phase, as obtained from (a) Monte Carlo simulations ($N = 27$, $a_0 = 0.8\ell_0$), and (b) the variational method. The bold lines indicate the positions of phase transitions and spinodals, compare Fig. 5.

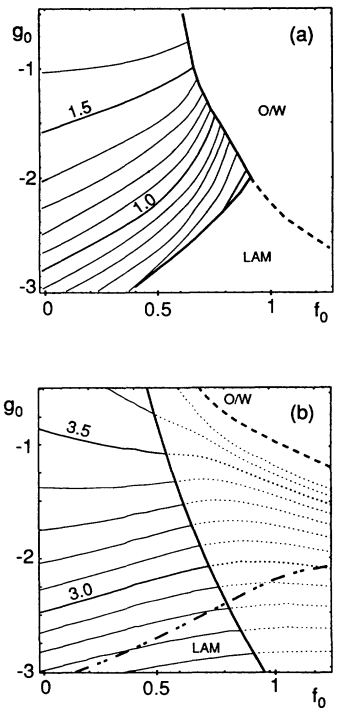

FIG. 12. Contour plot of the mean curvature squared $\langle H^2 \rangle$ of internal oil-water interfaces $(\Phi(\mathbf{r}) = 0)$ in the microemulsion or sponge phase, as obtained from (a) Monte Carlo simulations ($N = 27$, $a_0 = 0.8\ell_0$), and (b) the variational method. The bold lines indicate the positions of phase transitions and spinodals, compare Fig. 5.

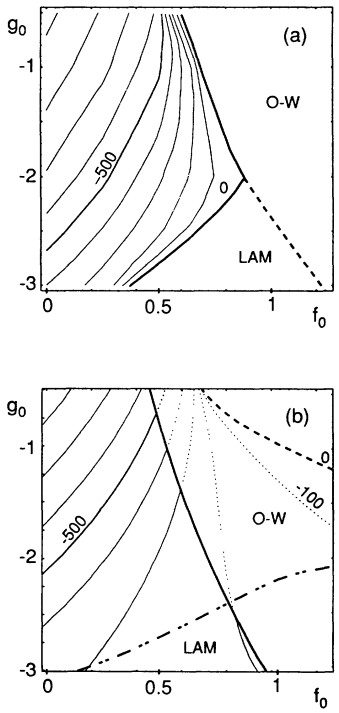

FIG. 13. Contour plot of the Euler characteristic χ_E of internal oil-water interfaces $[\Phi(\mathbf{r}) = 0]$ in the microemulsion or sponge phase, as obtained from (a) Monte Carlo simulations ($N = 27$, $a_0 = 0.8\ell_0$), and (b) the variational method. The bold lines indicate the positions of phase transitions and spinodals, compare Fig. 5.

$$\chi_E V^2/S^3 = -\pi/16 = -0.196$$

(Gaussian random fields) . (45)

Given the fact that the typical configurations of the order-parameter field look quite different, the similarity of these two values is quite surprising.

VIII. DISCUSSION

We have studied in this paper the thermal fluctuations of interfaces in microemulsions and sponge phases with the use of a simple Ginzburg-Landau model for ternary amphiphilic systems. We have employed Monte Carlo simulations, the variational method, and self-consistent perturbation theory to calculate the scattering intensities and correlation functions both in bulk and in film contrast, as well as the area S, the mean curvature squared $\langle H^2 \rangle$, and the Euler characteristic χ_E of the internal interfaces.

The self-consistent perturbation theory is unable to produce a strong peak in the scattering intensity with bulk contrast at the nonzero wave vector; it is thus limited in its application to weakly structured microemulsions. A comparison of the Monte Carlo method and the variational approach shows very good agreement for the scattering intensity in bulk contrast, for the phase transition between the microemulsion and the oil-rich and water-rich phases, and for the dimensionless ratio $\chi_E V^2/S^3$. This is a very useful result, since it indicates that in order to calculate phase diagrams of the Ginzburg-Landau model for other sets of parameters, time-consuming Monte Carlo simulations in search for phase transitions can be avoided. However, the variational approach fails for the scattering intensity in film contrast, and for the phase transition between microemulsion and lamellar phase. In particular, the variational approach is unable to produce a peak of the scattering intensity in film contrast at finite wave vector k. This is a serious deficiency of the Gaussian model. It shows that *level surfaces of Gaussian random fields do not accurately describe the structure of bicontinuous microemulsions.* The Monte Carlo results of our Ginzburg-Landau model, on the other hand, are in very good agreement with experimental results.

ACKNOWLEDGMENTS

Stimulating interactions with M. Kraus are greatfully acknowledged. We also thank R. Hausmann, M. Schick, and H. Wagner for helpful discussions. This work was supported in part by the Deutsche Forschungsgemeinschaft through Sonderforschungsbereich 266, and by Cray Research through the University Research & Development Grant Program.

[1] *Physics of Amphiphilic Layers*, edited by J. Meunier, D. Langevin, and N. Boccara, Springer Proceedings in Physics Vol. 21 (Springer, Berlin, 1987); *The Structure and Conformation of Amphiphilic Membranes*, edited by R. Lipowsky, D. Richter, and K. Kremer (Springer, Berlin, 1992); *Micelles, Membranes, Microemulsions, and Monolayers*, edited by W.M. Gelbart, D. Roux, and A. Ben-Shaul (Springer, Berlin, in press).

[2] G. Gompper and M. Schick, in *Phase Transitions and Critical Phenomena*, edited by C. Domb and J. Lebowitz (Academic Press, London, 1994), Vol. 16.

[3] G. Porte, J. Phys. Condens. Matter **4**, 8649 (1992).

[4] D. Roux, C. Coulon, and M.E. Cates, J. Phys. Chem. **96**, 4174 (1992).

[5] T. Hofsäss and H. Kleinert, J. Chem. Phys. **86**, 3565 (1987).

[6] D.A. Huse and S. Leibler, J. Phys. (Paris) **49**, 605 (1988).

[7] M. Teubner, J. Chem. Phys. **92**, 4501 (1990).

[8] K.R. Mecke and H. Wagner, J. Stat. Phys. **64**, 843 (1991).

[9] M. Teubner and R. Strey, J. Chem. Phys. **87**, 3195 (1987).

[10] G. Gompper and M. Schick, Phys. Rev. Lett. **65**, 1116 (1990).

[11] G. Gompper and M. Kraus, Phys. Rev. E **47**, 4289 (1993).

[12] G. Gompper, R. Hołyst, and M. Schick, Phys. Rev. A **43**, 3157 (1991).

[13] K. Putz, R. Hołyst, and M. Schick, Phys. Rev. A **46**, 3369 (1992).

[14] G. Gompper and S. Zschocke, Europhys. Lett. **16**, 731 (1991); Phys. Rev. A **46**, 4836 (1992).

[15] F. Schmid and M. Schick, Phys. Rev. E **49**, 494 (1994).

[16] G. Gompper and M. Hennes, Europhys. Lett. **25**, 193 (1994).

[17] G. Gompper and M. Kraus, Phys. Rev. E **47**, 4301 (1993).

[18] P. Pieruschka and S.A. Safran, Europhys. Lett. **22**, 625 (1993).

[19] K. Chen, C. Jayaprakash, R. Pandit, and W. Wenzel, Phys. Rev. Lett. **65**, 2736 (1990).

[20] J. Lerczak, M. Schick, and G. Gompper, Phys. Rev. A **46**, 985 (1992).

[21] M.E. Cates, D. Roux, D. Andelman, S.T. Milner, and S.A. Safran, Europhys. Lett. **5**, 733 (1988).

[22] D. Roux, M.E. Cates, U. Olsson, R.C. Ball, F. Nallet, and A.M. Bellocq, Europhys. Lett. **11**, 229 (1990).

[23] G. Gompper and M. Schick, Phys. Rev. E **49**, 1478 (1994).

[24] K. Mecke, Diplomarbeit, Universität München, 1989 (unpublished).

[25] There are several possibilities to define the Euler characteristic on the lattice, depending on how the surfaces which touch at edges or corners are treated [24]. We use here a symmetrized version, where in these cases the surfaces are counted as connected and disconnected with probability 1/2. Another possibility is discussed in Ref. [5].

[26] H.S. Seung and D.R. Nelson, Phys. Rev. A **38**, 1005 (1988).

[27] D.M. Kroll and G. Gompper, Science **255**, 968 (1992).

[28] K. Binder and D.W. Heermann, *Monte Carlo Simulation in Statistical Physics*, Springer Series in Solid State Sciences Vol. 80 (Springer-Verlag, Berlin, 1988).
[29] R.P. Feynman, Phys. Rev. **97**, 660 (1955); R.P. Feynman and A.R. Hibbs, *Quantum Mechanics and Path Integrals* (McGraw-Hill, New York, 1965).
[30] N.F. Berk, Phys. Rev. Lett. **58**, 2718 (1987); Phys. Rev. A **44**, 5069 (1991).
[31] M. Teubner, Europhys. Lett. **14**, 403 (1991).
[32] P. Pieruschka and S. Marčelja, J. Phys. II **2**, 235 (1992).
[33] The generalization of these results to the case $\langle\Phi\rangle = \bar{\Phi}$ is straightforward.
[34] Y. Levin, C.J. Mundy, and K.A. Dawson, Phys. Rev. A **45**, 7309 (1992).
[35] F.A. Lindemann, Phys. Z. **11**, 609 (1910).
[36] S.-H. Chen, S.-L. Chang, and R. Strey, J. Chem. Phys. **93**, 1907 (1990); J. Appl. Crystallogr. **24**, 72 (1991).
[37] B. Widom, J. Chem. Phys. **90**, 2437 (1989).
[38] G. Gompper and M. Schick, Phys. Rev. A **42**, 2137 (1990).
[39] M.W. Matsen and D.E. Sullivan, Phys. Rev. A **44**, 3710 (1991).
[40] In the one-dimensional lattice models studied in Refs. [38] and [39], the wavelengths of the film and the order-parameter correlation functions are unrelated. In the three-dimensional case, the wavelength of order-parameter correlation function is exactly *twice* as large as the wavelength of the film correlation function.
[41] K.-V. Schubert and R. Strey, J. Chem. Phys. **95**, 8532 (1991).
[42] M. Skouri, J. Marignan, J. Appell, and G. Porte, J. Phys. II **1**, 1121 (1991).
[43] R. Strey, J. Winkler, and L. Magid, J. Phys. Chem. **95**, 7502 (1991).

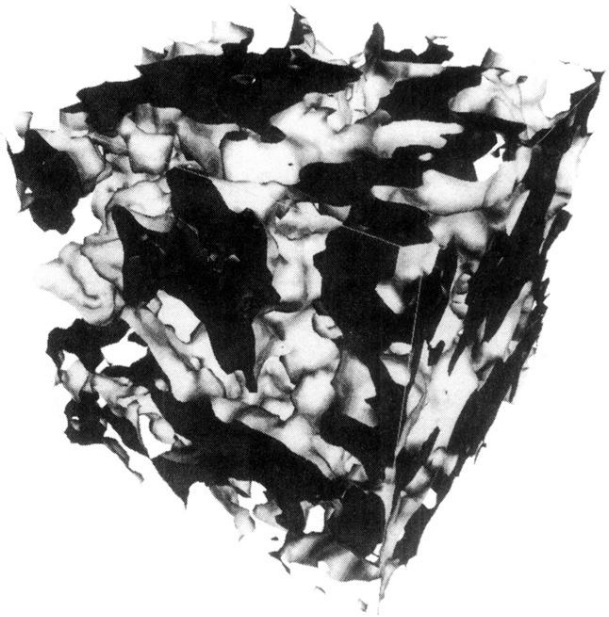

FIG. 10. Typical configuration of the $\Phi(\mathbf{r}) = 0$ surfaces in a microemulsion. The parameters are $g_0 = -2.0$, $f_0 = 0.75$, $a_0 = 0.6\ell_0$, and $N = 45$. The figure shows only a part (of size $36 \times 36 \times 36$) of the total lattice. The two sides of the interface are colored differently, dark on the oil-rich side, light on the water-rich side.